2018

Suppression of the photocatalytic activity of TiO2 nanoparticles encapsulated by chitosan through a spray-drying method with potential for use in sunblocking applications

Alexander Morlando
University of Wollongong, am700@uowmail.edu.au

Vitor Sencadas
University of Wollongong, victors@uow.edu.au

Dean Cardillo
University of Wollongong, dwc583@uowmail.edu.au

Konstantin K. Konstantinov
University of Wollongong, konstan@uow.edu.au

Publication Details

Morlando, A., Sencadas, V., Cardillo, D. & Konstantinov, K. (2018). Suppression of the photocatalytic activity of TiO2 nanoparticles encapsulated by chitosan through a spray-drying method with potential for use in sunblocking applications. Powder Technology, 329 252-259.

Suppression of the photocatalytic activity of TiO2 nanoparticles encapsulated by chitosan through a spray-drying method with potential for use in sunblocking applications

Abstract

Solar exposure, in particular to UVA and UVB radiation, is a major carcinogen through direct DNA damage and the production of reactive oxygen species (ROS). Inorganic UV filters present in sunscreening agents, such as titanium dioxide (TiO 2), are commonly employed for protection however, due to their photocatalytic nature, they have been shown to instigate the production of ROS when irradiated with UV radiation, which in turn can lead to the degradation of the sunscreening formulation and subsequent damage to the skin. In this work, chitosan/TiO 2 nanocomposite particles were produced via a spray-drying method, in a single step, directly through aqueous solution for the purpose of reducing the photocatalytic activity of commercially available TiO 2 nanoparticles. The photocatalytic activity of the nanocomposite materials were assessed using the organic dye, crystal violet, as the degradation target and irradiating in a UV reactor. It was found that the photoactivity of the chitosan encapsulated nanoparticles were greatly reduced compared to that of the pristine TiO 2 nanoparticles, from 95% degradation after 120 min for pristine TiO 2 to 39.5% for the chitosan/TiO 2 spray dried particles, highlighting the potential for this simple coating process and chitosan material for application as an inactive protective coating for sunblocking applications.

Disciplines

Engineering | Physical Sciences and Mathematics

Publication Details

Morlando, A., Sencadas, V., Cardillo, D. & Konstantinov, K. (2018). Suppression of the photocatalytic activity of TiO2 nanoparticles encapsulated by chitosan through a spray-drying method with potential for use in sunblocking applications. Powder Technology, 329 252-259.

Suppression of the photocatalytic activity of TiO_2 nanoparticles encapsulated by chitosan through a spray-drying method with potential for use in sunblocking applications

Alexander Morlando[a], Vitor Sencadas[b,c,], Dean Cardillo[a] and Konstantin Konstantinov[a,*]*

Affiliations
[a]Institute for Superconducting and Electronic Materials, AIIM Facility, University of Wollongong Innovation Campus, Squires Way, North Wollongong, NSW 2500, Australia.
[b]School of Mechanical, Materials and Mechatronic Engineering, Faculty of Engineering and Information Science, University of Wollongong, Wollongong, NSW 2522, Australia.
[c]ARC Centre of Excellence for Electromaterials Science, University of Wollongong, NSW 2522, Australia.

*Corresponding Authors:
Dr. Konstantin Konstantinov
Email: konstan@uow.edu.au
Tel: +61 24221 5765; Fax: +61 24221 5731
Dr. Vitor Sencadas
Email: victors@uow.edu.au

Abstract

Solar exposure, in particular to UVA and UVB radiation, is a major carcinogen through direct DNA damage and the production of reactive oxygen species (ROS). Inorganic UV filters present in sunscreening agents, such as titanium dioxide (TiO_2), are commonly employed for protection however, due to their photocatalytic nature, they have been shown to instigate the production of ROS when irradiated with UV radiation, which in turn can lead to the degradation of the sunscreening formulation and subsequent damage to the skin. In this work, chitosan/TiO_2 nanocomposite particles were produced via a spray-drying method, in a single step, directly through aqueous solution for the purpose of reducing the photocatalytic activity of commercially available TiO_2 nanoparticles. The photocatalytic activity of the nanocomposite materials were assessed using the organic dye, crystal violet, as the degradation target and irradiating in a UV reactor. It was found that the photoactivity of the chitosan encapsulated nanoparticles were greatly reduced compared to that of the pristine TiO_2 nanoparticles, from 95% degradation after 120 min for pristine TiO_2 to 39.5% for the chitosan/TiO_2 spray dried particles, highlighting the potential for this simple coating process and chitosan material for application as an inactive protective coating for sunblocking applications.

Keywords

Chitosan; Thermal properties; Optical properties; Photocatalysis; UV filtration

https://doi.org/10.1016/j.powtec.2018.01.057

1. Introduction

Solar UV radiation exposure, particularly to wavelengths in the UVA (320 - 400 nm) and UVB (290 - 320 nm) regions, is a known cause of skin cancers and has been proven to cause DNA damage both directly and indirectly through the production of reactive oxygen species (ROS) and induction of oxidative stress [1]. The use of UV filtering products such as sunscreens is the primary means of protection employed. These products contain organic and inorganic compounds, which can protect the skin against UV radiation through modes of absorption, scattering or reflection. Titanium dioxide (TiO_2) is extensively used in sunscreen products as an inorganic UV filter due to its broadband protection across the UVA and UVB regions, as well as its ability to produce high sun protection factor (SPF) products. Additionally, modern sunscreen products may now contain this material in the form of nanoparticles, not only due to the increased transparency in formulation, but also due to the increased absorbance of UV radiation they display comparatively to larger particles as a result of size quantization [2]. TiO_2 is a semiconducting material which, when illuminated by electromagnetic radiation of energy equal to or greater than its band gap (E_g), can result in the production of photoexcited electron (e^-)/ hole (h^+) pairs. In the context of a biological system, these photoexcited species can interact with molecules adsorbed to the surface of these particles such as water (H_2O), a major constituent of human cells, producing ROS, which can go on to cause cellular and potentially mutagenic damage. Some of these ROS include hydroxyl ($OH^{\cdot}$) and superoxide ($O^{2-\cdot}$**)** radicals and are due to interfacial redox reactions between the e^-/h^+ pairs and adsorbed H_2O molecules. One study on the photoxidative ability of these photocatalysts involved the investigation of various sunscreen products containing TiO_2 and the effect when applied to steel sheets pre-painted with highly durable coatings such as fluoropolymer coating types [3]. After performing a series of "accelerated weathering" experiments, it was found that formulations containing these inorganic components resulted in severe degradation of the panels in terms of gloss and surface roughness. In addition, it was found through X-ray diffraction that, for a particular cream, the active UV filtering TiO_2 ingredient shared a similar mixed anatase/rutile crystal structure to that of the known commercial photocatalyst TiO_2 powder (P25). This commercial powder has been extensively studied for use in applications such as dye-sensitized solar cells, self-cleaning glass and water purification owing to its photocatalytic nature and ability to generate free-radicals [4-6]. As such, despite the inherent benefits of nanoparticles in sunscreen products, there has been concern as to the potential of these materials to penetrate past the skin and to induce oxidative stress due to their known photocatalytic activity. In a review on the safety of nanoparticles in sunscreens [7], it was concluded that the

https://doi.org/10.1016/j.powtec.2018.01.057

weight of evidence suggests that these nanoparticles remain on the surface of the skin and the outer layer of the stratum corneum, where they can only interact with non-viable cells, however there is conclusive *in vitro* evidence that, whilst in the presence of UV radiation, these materials are able to produce ROS, which can potentially lead to the damaging of cells. Furthermore, it has been suggested by the Scientific Committee on Consumer safety (SCCS) that highly photoactive or easily inhalable spray or cream products containing TiO_2 nanoparticle should not be used [8]. As such, there has been an emphasis on developing and investigating alternative materials for potential use as UV filtering additives in sunscreen products. Some potential candidates include cerium oxide CeO_2, iron oxide (Fe_2O_3) and tin oxide (SnO_2) [9-11]. Developing methods for reducing the production of ROS and thus reducing the photocatalytic activity of TiO_2 is an additional approach being explored and include methods of doping with foreign elements and coating/encapsulating with ceramic or polymeric materials. Wakefield *et al* synthesized manganese (Mn) doped TiO_2 nanoparticles through a sol gel method with increased UVA attenuation [12]. Additionally, the free radical production was observed to be inhibited and was attributed to a free radical scavenging effect. Commonly used coating materials include wide Eg metal oxides, such as silica (SiO_2) [13] and alumina (Al_2O_3) [14] however, conflicting reports have shown that such composites could in fact enhance the photoactivity [15], thus alternative materials such as polymers have also been investigated [16]. One promising coating/encapsulating material is the natural polymer chitosan. Chitosan is a non-toxic, biocompatible and biodegradable polysaccharide that has gained interest for use in biomedical applications such as drug delivery, artificial skin and wound dressing [17-19]. Studies involving chitosan as a coating material have also been reported and have yielded promising results in the context of UV filtration. For example, an investigation into the photocatalytic activity of chitosan/ZnO composite nanoparticles synthesized through ionotropic gelation had been investigated and reported to exhibit a quenching effect on the free radical production of ZnO [20] highlighting its potential suitability for use as a UV filtering additive in cosmetic products. Work on the development of chitosan/TiO_2 composites has been reported but such findings generally involve chitosan as a form of scaffolding for the TiO_2 usually for tissue engineering [21] and ultrafiltration [22] applications. In this study, nanocomposite chitosan/TiO_2 particles were processed by spray drying, in a single step, and an investigation into the optical, thermal and morphological properties of the composite materials was carried out. Additionally, the effect of chitosan as a coating on the photocatalytic activity of the TiO_2 core nanoparticles was assessed through the photodegradation of an organic dye, crystal violet (CV), in the presence of the synthesized materials.

2. Materials and Methods

https://doi.org/10.1016/j.powtec.2018.01.057

2.1 Synthesis of chitosan and chitosan/TiO_2 particles

For the preparation of the chitosan and chitosan/TiO_2 (denoted CHI and CHI/TiO_2 here forth) nanocomposite materials, desired quantities of chitosan powder (from Shrimp shells, ≥75% deacetylated, Sigma Aldrich) and commercial photocatalyst TiO_2 powder (P25, Degussa Evonik) were weighed and transferred to a beaker containing a solution of 3% v/v aqueous acetic acid (CH_3COOH, Sigma Aldrich) in deionized water such that the theoretical weight ratios of chitosan to TiO_2 were 2:1, 1:1 and 1:0 (in the case of the purely chitosan sample). The solution was left to stir overnight so as to ensure homogeneity before being spray-dried through a 0.7 mm spray drying nozzle using a home-made spray dryer system at a flow rate of 100 mL hr^{-1} with an inlet temperature of 120^{o}C and outlet temperature of 40^{o}C. The resultant CHI and CHI/TiO_2 nanocomposite particles were cross-linked via a vapour phase process using a heated vacuum desiccator system (JP Selecta S.A.) set at 25^{o}C and in the presence of glutaraldehyde ($OHC(CH_2)_3CHO$, 50% in H_2O, Sigma Aldrich) for 48 hrs.

2. 2 Materials Characterization

Scanning electron microscopy was performed on the CHI and CHI/TiO_2 nanocomposite particles by initially immobilizing on an SEM stage using double-sided carbon tape and coated with platinum before being analysed using an JSM-7500FA field emission electron microscope with a Bruker X-Flash 4010 10 mm^2 X-ray detector for energy dispersive X-ray mapping images. The average diameter and distribution of the nanocomposite particles were calculated over approximately 50 particles using the Image-J software. In addition, transmission electron micrographs were obtained using a JEM-2010 transmission electron microscope (JEOL) on low concentration samples drop cast onto lacey/carbon 200 meshes. X-ray diffraction patterns for the pristine chitosan, TiO_2 and nanocomposite particles were obtained using a MAC Science X-ray diffractometer scanning between $2\theta = 4 – 60^{o}$ at a scan speed of 1.5^{o} min^{-1} and step size of 0.020. Thermo-gravimetric analysis (TGA) was performed using a Mettler-Toledo TGA/DSC in the temperature range of 40 – 800 ^{o}C at varying heating rates (between 10 and 40 ^{o}C min^{-1}) under regular atmospheric air. Fourier transform infrared spectra (FTIR) were collected with a Shimadzu IRAffinity-1 FTIR coupled with a Miracle 10 total reflection attachment (Shimadzu Scientific Instruments) scanning between the wavelengths of 600 - 4000 cm^{-1} at a resolution of 2 cm^{-1}. Diffuse reflectance spectra were collected on the powdered samples using a UV-3600 Spectrophotometer (Shimadzu) coupled with an integrating sphere attachment (Shimadzu ISR-3100) scanning in the range of 300 - 800 nm.

2.3 Assessment of photocatalytic activity towards degradation of crystal violet

https://doi.org/10.1016/j.powtec.2018.01.057

The photocatalytic activity of the composite samples were evaluated using the water soluble dye, crystal violet (CV, dye content ≥90%, Sigma Aldrich), as a decomposition target. A RPR-200 Photochemical Reactor (Rayonet) lined with 300 nm (8x, 21 W) and 350 nm (8x, 24 W) phosphor-coated lamps were used as the irradiation source. A 100 mL suspension of the composite particles (5 mg L^{-1}) in a solution of the dye (5 mg L^{-1}) was created and transferred to a quartz beaker and left to stir under darkness in the photoreactor for 30 min. The mixture was then irradiated for a period of 2hr and 10 mL aliquots collected periodically every 20 min. The resultant degradation was assessed via UV-Vis spectroscopy using a UV-1800 Spectrophotometer (Shimadzu) by measuring the changes in the major absorption peak of the dye at λ = 590 nm.

3. Results and Discussion

3.1 Synthesis setup and microstructural analysis

The setup used for the spray drying system is represented in Fig. 1. Briefly, the solution is fed to the nozzle with the aid of a peristaltic pump. The nozzle is connected to an air pump system that atomizes the solution, while a hot air stream is applied in co-current flow, leading to the drying of the polymer nanocomposite droplets, and subsequently to the solid particle formation.

SEM/TEM micrographs of the chitosan/TiO_2 composites were obtained so as to ascertain the morphological profile of the spray dried particles and to assess the loading effects on the particle sizes obtained. As highlighted from SEM (Fig. 2) and TEM (Fig. S1), the TiO_2 loading amount has an impact on the particle morphology and particle sizes of the spray-dried composite particles. In absence of the TiO_2 nanoparticles, the CHI particles formed are spherical and symmetric in shape but relatively inhomogeneous in size. With the incorporation of the TiO_2 nanoparticles, it is evident there is an increase in the size of the composite particles formed and, whilst still primarily spherical, the surfaces of the particles appear deformed and rough due to the presence of TiO_2 decorating the outer layer of the polymer shell. This surface roughness is much more evident in the case of the 1:1 CHI/TiO_2 sample due to the higher ceramic particle loading, relative to the 2:1 CHI/TiO_2 sample.

In addition to the change in particle morphology it can be seen through TEM (Fig. S1) of the 1:1 CHI/TiO_2 sample regions in which the ceramic nanofiller decorates the external layer of the polymer matrix that perhaps suggests an optimal loading amount exists between the 1:1 and 2:1 CHI/TiO_2 samples. The particle diameters were measured from the SEM images obtained and the mean values listed in Table 1 along with their corresponding coefficient of variation (COV). It was observed that the average particle diameter increases with the amount of TiO_2 nanoparticles incorporated in the aqueous spray solution (Table 1). Furthermore, CHI had an average particle diameter of 1.40 ± 0.4,

and an increase of more than one-fold (2.5 ± 0.3 was observed for the sample with the highest TiO_2 nanoparticle content. Further characterization of the positioning of the encapsulated TiO_2 nanoparticles was performed using an energy dispersive spectroscopic (EDS) mapping technique. Fig. 2(right) highlights the distribution of titanium (Ti) throughout the spray-dried chitosan particles. For the purely chitosan sample (Fig. 2a)), the mapping of Ti resulted in a random distribution, indicating no localized concentration of Ti atoms in the CHI particles and is attributed to general background noise. For the composite samples (Fig. 2b) and c)), a consistent distribution of Ti atoms are concentrated and localized within the particles positioned in the foreground and background of the corresponding grey-scale images, suggesting that the spray-drying technique was a successful approach to encapsulate the core TiO_2 nanoparticles.

Fig. 3 highlights the XRD patterns obtained for the pristine TiO_2 nanoparticles, chitosan microparticles and the nanocomposite particles. The chitosan microparticles exhibit a broad diffraction peak around 20^o, corresponding to the crystalline structure-II [23, 24]. Moreover, the diffraction pattern of the pristine TiO_2 nanoparticles suggest a mixture of the anatase and rutile crystal phases of TiO_2, with the major peaks for each phase appearing at $2\theta = 25^o$ and 27^o [25]. For the nanocomposite microparticles, no clear changes in the diffraction patterns was noticed when compared to the pristine raw materials (ceramic nanopowder and chitosan), suggesting that the chitosan encapsulation or the processing method has no effect on the crystal phase of the incorporated TiO_2 nanoparticles.

3.2 Chemical and thermal characterization

Fig. 4 displays the FTIR spectra obtained for the spray-dried chitosan and nanocomposite particles, as well as the pristine TiO_2 nanoparticles. In the case of the chitosan containing materials, characteristic peaks may be observed including absorption bands between 3305 - 3280 cm^{-1}; 2888 - 2875 cm^{-1}; 1558 - 1550 cm^{-1}; 1421 - 1410 cm^{-1} and 1065 - 1050 cm^{-1} corresponding to -OH; -C-H; -NH; -CH; and C-O vibrational modes [23, 26]. In addition to these characteristic bands, an absorption band can also be observed in all chitosan containing samples in the range of 1652 - 1645 cm^{-1} which is associated with the amide II carbonyl stretch of the chitosan precursor structure, chitin (Fig. S3) [27, 28], and is to be expected considering the starting raw chitosan material consisted of a deacetylation degree of ≥75%. The presence of the TiO_2 in the composite materials is also further supported due to the occurrence of strong Ti-O stretch bands (627 - 610 cm^{-1}) in both the 2:1 and 1:1 composite samples, coinciding with the same absorption band reported in the pristine TiO_2 spectrum, and corroborates with the results obtained through SEM-EDS (Fig. 2).

Thermal degradation of the chitosan and TiO_2/chitosan nanocomposites was assessed by thermogravimetric analysis (TGA). Aqueos spray-dried chitosan particles presented three main weight loss steps (Fig. 5a) and b)). The first occurs between 40 – 110 ^{o}C, corresponding to a weight loss of 5.5% and is attributed to the loss of unbonded and adsorbed water, due to the hydrophilic nature of chitosan. The second step occurs between 220 – 350 ^{o}C, from which a further loss of 40.5% is observed. This weight loss is often attributed to the random splitting of the chitosan polysaccharide structure during decomposition and the removal of degradation by-products such as acetic, butyric and low mass fatty acids [29, 30]. The final stage, occurring between 350 – 750 ^{o}C, arises from the presence of residual cross-linked chitosan chains [31] and is connected with the remaining sample weight loss (45.6%), leaving a residual mass of 9% (Table 1). The onset of degradation (T_{onset}) for the 2:1 (228 ^{o}C) and 1:1 (236 ^{o}C) CHI/TiO_2 samples occurs earlier than that of the CHI sample (269^{o}C) suggesting that the incorporation of the inorganic TiO_2 nanoparticles leads to a decrease in the nanocomposites thermal stability, and is likely due to the thermal conductivity of the ceramic TiO_2 nanoparticles (Fig. 5 a) and b)), resulting in a homogenous distribution of heat supplied to the sample. As with the CHI sample, the second degradation stage, corresponding to the decomposition of cross-linked chitosan chains, also appears in the nanocomposite samples. Additionally, the decomposition of the chitosan component of the nanocomposite samples appears to end at a lower temperature (c.a. 585^{o}C) than that of the purely chitosan sample (725^{o}C), further highlighting the reduced thermal stability of the nanocomposite materials.

The activation energy (E_a) for the onset of decomposition for the spray-dried chitosan and nanocomposite samples was calculated using the Kissinger model:

$$\ln\left(\frac{\beta}{T_p^2}\right) = \frac{\ln(AE_a)}{R} + \ln[n(1-\alpha_p)^{1-n} - \frac{E_a}{RT_p} \quad (1)$$

where A is the pre-exponential factor (min^{-1}), R the ideal gas constant (8.31 J mol^{-1} K^{-1}), β the heating rate and α_p and T_p the degree of conversion and temperature at the maximum weight loss [32]. From the plot of $\ln(\beta/T^2_p)$ against $1/T_p$, at heating rates between 10 and 40 ^{o}C min^{-1}, the E_a can be calculated from the slope of the line produced (Fig. 5c)). The values obtained for the spray-dried chitosan and composite samples are listed in Table 1 and correlate with the initial onset of degradation for the spray-dried samples, in that, the CHI sample displays the highest degree of thermal stability (E_a = 183 kJ mol^{-1}) followed by the 1:1 (E_a = 119 kJ mol^{-1}) and the 2:1 (E_a = 95 kJ mol^{-1}) CHI/TiO_2 samples. The loading ratios for the composite particles were also estimated from the 20^{o}C min^{-1} TGA curve (Fig. 5a)) obtained by subtracting the residual mass percentage of the purely chitosan sample from those of the composite samples. In this way, the percentage of TiO_2 in the

https://doi.org/10.1016/j.powtec.2018.01.057

composite samples were determined to be 32% (2:1 CHI/TiO_2) and 47% (1:1 CHI/TiO_2), which agrees with the desired loading amounts.

3.3 UV-Vis Diffuse reflectance studies

Diffuse reflectance spectra were obtained to ascertain the effect of the chitosan on the optical properties of the encapsulated TiO_2 nanoparticles. Fig. 6a) highlights the absorption spectra obtained for the nanocomposite particles as well as the purely chitosan particles and pristine TiO_2 nanoparticles. In the case of the TiO_2 nanoparticles, the absorption edge for the material begins at 405 nm and plateaus at 310 nm, corresponding to the UVB region [33]. For the CHI sample, the primary absorption band is observed in the UV region and plateaus at 305 nm, however, steady absorption is observed across the visible light region, with smaller absorption peaks seen at 445 nm, 525 nm and 665 nm (Fig. 6a)). The absorption features seen at 305 nm, 445 nm and 525 nm could be attributed to electronic transitions occurring from $\sigma \rightarrow \sigma^*$and $\pi \rightarrow \pi^*$ molecular orbitals [34] owing to the mixture of sp^3 and sp^2 hybridized bonds present as a result of the less than 100% deacetylation degree of the chitosan. Transitions occurring from non-bonding (n) orbitals may also arise due to the presence of atoms such as oxygen and nitrogen in the chitosan structure that have lone pairs of electrons capable of undergoing such transitions [35, 36] , and could explain the appearance of the absorption peak at 665 nm as being a $n \rightarrow \pi^*$ transition. In the case of the nanocomposite materials, we can see that the UV absorption edges appear red-shifted compared to the pristine TiO_2 nanoparticles, with broad absorption bands plateauing between 320 - 325 nm, within the UVA region. In addition to the shift into the UVA region, translation of pure chitosan visible light absorption features can also be observed, with the features being more prominent in the case of the 2:1 CHI/TiO_2 sample due to the higher concentration of chitosan present. Further, the pale yellow appearance brought about by the chitosan absorption features could be appealing in cosmetic cream formulations due to the closer appearance to skin tones.

3.4 Assessment of photocatalytic activity

The photocatalytic activity of the spray-dried chitosan, nanocomposite particles and the pristine TiO_2 nanoparticles, were evaluated by measuring the degradation of CV under UV irradiation over a period of 2 hr. Previous work has shown that the degradation of such dyes follow a pseudo first order rate mechanism following the Langmuir-Hinshelwood model [37]. Simplifying the model when the initial concentration of the dye C_o is low, as in this case, yields the following expression:

$$\ln\left(\frac{C_o}{C}\right) = kt \tag{2}$$

where *t* is the irradiation time (min), *C* the concentration (mg L^{-1}) and *k* the apparent first order rate constant (min^{-1}).

Fig. 6b), Fig. 7 and Table 2 highlight the photodegradation efficiencies, kinetics plots and rate constants for the degradation of the CV dye after UV irradiance in the presence of the as-prepared materials. It is clear that the incorporation of the chitosan layer in the nanocomposite particles significantly impacts the degradation efficiency of the TiO_2 nanoparticles. It can be seen that the photocatalytic activity of the TiO_2 is hindered, and the degradation efficiency decreases in accordance with the content of chitosan, whereby, the pristine TiO_2 nanoparticles display the highest degradation efficiency (95.7%) followed by the 1:1 (58.3%), 2:1 (39.5%) CHI/TiO_2 and CHI (15.5%) samples (Table 2). A possible reason for the substantial decrease in photocatalytic activity of the composite materials could be associated with the inhibition of free-radical production due to the external layer of chitosan polymer [20]. It has been previously reported [38, 39] that the application of an inert coating layer to photocatalytic metal oxide particles can act as a means of blocking the migration of photogenerated charge carriers to the surface of the excited particle, thus preventing interfacial charge transfer reactions from occurring. Another factor affecting the reduced degradation rates for the composite materials could also be the agglomeration of the encapsulated TiO_2 particles, thus reducing the total surface area available for chemical adsorption of the CV dye molecules. This in turn reduces the efficiency of the dye degradation due to the lower concentration of chemically adsorbed CV molecules as a result of the TiO_2 nanoparticle packing [40, 41]. Kinetics plots (Fig. S5) were calculated and obtained so as to obtain the apparent rate constant, *k*, for each the degradation of CV in the presence of the as-prepared materials (Table 2 and Fig. 6b)). Comparing the two nanocomposite samples, the increased degradation rate for the 1:1 CHI/TiO_2 ($7.3\pm0.5 \times 10^{-3}$ min^{-1}) sample relative to the 2:1 CHI/ TiO_2 ($4.2\pm0.2 \times 10^{-3}$ min^{-1}) sample coincides with the greater presence of surface TiO_2nanoparticles decorating the chitosan outer layer, as evidenced in Fig. 2. The greatly reduced photoactivity of these composite materials relative to the photocatalytic TiO_2 nanoparticles, combined with the slight red-shift in UV protection, further highlights the potential for chitosan as a potential biocompatible coating agent for inorganic TiO_2 nanoparticles used in sunscreen products.

4. Conclusions

Chitosan and chitosan/TiO_2 nanocomposite particles were successfully produced through the use of a spray-drying technique and evaluated for the possible application of chitosan as a coating agent for inorganic TiO_2 nanoparticles in UV filtering applications. The morphology and mean particle sizes of the synthesized materials were characterized through the use of SEM and TEM micrographs and

showed that an increase in TiO_2 loading yields an expansion in mean particle size as well as presence of surface TiO_2 particles when the loading exceeds the capacitive amount for the spray-dried chitosan particles. The thermal properties of the chitosan and composite samples were analysed using TGA/DTA methods and showed that the thermal stability of the composites was decreased relative to that of the purely chitosan sample, whilst FTIR analysis displayed absorption peaks corresponding to characteristic chitosan and TiO_2 vibrational modes in the case of the composite particles. Diffuse reflectance spectra for the synthesized materials and pristine TiO_2 nanoparticles were obtained and showed that the primary UV absorbance band in the composite samples was slightly red-shifted into the UVA region whilst also displaying additional, smaller, visible light region absorption peaks as a result of the chitosan coating leading to a pale-yellow tone for the composite powders. The photocatalytic activity of the spray-dried materials were evaluated and the activity of the composite chitosan/TiO_2 particles was found to be significantly reduced in comparison to that of the unbound TiO_2 nanoparticles, highlighting the potential for this chitosan coating process for use in the industrial manufacturing of inorganic TiO_2 containing sunscreen products.

Acknowledgements

This research has been conducted with the support of the Australian Government Research Training Program Scholarship. The author additionally acknowledges the use of the facilities within the Australian National Fabrication Facility Node as well as the use of the facilities and the assistance of Dr. Gilberto Casillas Garcia at the University of Wollongong Electron Microscopy Center.

References

[1] M. Ichihashi, M. Ueda, A. Budiyanto, T. Bito, M. Oka, M. Fukunaga, K. Tsuru, T. Horikawa, UV-induced skin damage, Toxicology, 189 (2003) 21-39.
[2] G.P. Dransfield, Inorganic Sunscreens, Radiation Protection Dosimetry, 91 (2000) 271-273.
[3] P.J. Barker, A. Branch, The interaction of modern sunscreen formulations with surface coatings, Progress in Organic Coatings, 62 (2008) 313-320.
[4] C. Belver, J. Bedia, M.A. Álvarez-Montero, J.J. Rodriguez, Solar photocatalytic purification of water with Ce-doped TiO2/clay heterostructures, Catalysis Today, 266 (2016) 36-45.
[5] U. Bach, D. Lupo, P. Comte, J.E. Moser, F. Weissortel, J. Salbeck, H. Spreitzer, M. Gratzel, Solid-state dye-sensitized mesoporous TiO2 solar cells with high photon-to-electron conversion efficiencies, Nature, 395 (1998) 583-585.
[6] S.M. Kim, I. In, S.Y. Park, Study of photo-induced hydrophilicity and self-cleaning property of glass surfaces immobilized with TiO2 nanoparticles using catechol chemistry, Surface and Coatings Technology, 294 (2016) 75-82.
[7] T.G. Administration, Literature review on the safety of titanium dioxide and zinc oxide nanoparticles in sunscreens, Therapeutic Goods Administration, Australian Government, Department of Health, 2016.

[8] Sccs, Q. Chaudhry, Opinion of the Scientific Committee on Consumer safety (SCCS) – Revision of the opinion on the safety of the use of titanium dioxide, nano form, in cosmetic products, Regulatory Toxicology and Pharmacology, 73 (2015) 669-670.
[9] F. Caputo, M. De Nicola, A. Sienkiewicz, A. Giovanetti, I. Bejarano, S. Licoccia, E. Traversa, L. Ghibelli, Cerium oxide nanoparticles, combining antioxidant and UV shielding properties, prevent UV-induced cell damage and mutagenesis, Nanoscale, 7 (2015) 15643-15656.
[10] D. Cardillo, M. Weiss, M. Tehei, T. Devers, A. Rosenfeld, K. Konstantinov, Multifunctional Fe 2 O 3/CeO 2 nanocomposites for free radical scavenging ultraviolet protection, RSC Advances, 6 (2016) 65397-65402.
[11] A. Morlando, D. Cardillo, T. Devers, K. Konstantinov, Titanium doped tin dioxide as potential UV filter with low photocatalytic activity for sunscreen products, Materials Letters, 171 (2016) 289-292.
[12] G. Wakefield, S. Lipscomb, E. Holland, J. Knowland, The effects of manganese doping on UVA absorption and free radical generation of micronised titanium dioxide and its consequences for the photostability of UVA absorbing organic sunscreen components, Photochemical & Photobiological Sciences, 3 (2004) 648-652.
[13] H.-H. Ko, H.-T. Chen, F.-L. Yen, W.-C. Lu, C.-W. Kuo, M.-C. Wang, Preparation of TiO2 nanocrystallite powders coated with 9 mol% ZnO for cosmetic applications in sunscreens, International journal of molecular sciences, 13 (2012) 1658-1669.
[14] F. Bertrand, S.-A. German, A. Anwar, V. Irune, B. Gemma, R.D.M. Yolanda, B. Lennart, Dispersion and surface functionalization of oxide nanoparticles for transparent photocatalytic and, Science and Technology of Advanced Materials, 14 (2013) 023001.
[15] R. Dunford, A. Salinaro, L. Cai, N. Serpone, S. Horikoshi, H. Hidaka, J. Knowland, Chemical oxidation and DNA damage catalysed by inorganic sunscreen ingredients, FEBS letters, 418 (1997) 87-90.
[16] B. Seentrakoon, B. Junhasavasdikul, W. Chavasiri, Enhanced UV-protection and antibacterial properties of natural rubber/rutile-TiO 2 nanocomposites, Polymer degradation and stability, 98 (2013) 566-578.
[17] A. Bernkop-Schnürch, S. Dünnhaupt, Chitosan-based drug delivery systems, European Journal of Pharmaceutics and Biopharmaceutics, 81 (2012) 463-469.
[18] R. Jayakumar, M. Prabaharan, P.S. Kumar, S. Nair, H. Tamura, Biomaterials based on chitin and chitosan in wound dressing applications, Biotechnology advances, 29 (2011) 322-337.
[19] S. Parvez, M.M. Rahman, M.A. Khan, M.A.H. Khan, J.M. Islam, M. Ahmed, M.F. Rahman, B. Ahmed, Preparation and characterization of artificial skin using chitosan and gelatin composites for potential biomedical application, Polymer Bulletin, (2012) 1-17.
[20] A. Regiel-Futyra, M. Kus-Liśkiewicz, S. Wojtyła, G. Stochel, W. Macyk, The quenching effect of chitosan crosslinking on ZnO nanoparticles photocatalytic activity, RSC Advances, 5 (2015) 80089-80097.
[21] R. Jayakumar, R. Ramachandran, V. Divyarani, K. Chennazhi, H. Tamura, S. Nair, Fabrication of chitin–chitosan/nano TiO 2-composite scaffolds for tissue engineering applications, International journal of biological macromolecules, 48 (2011) 336-344.
[22] D. Yang, J. Li, Z. Jiang, L. Lu, X. Chen, Chitosan/TiO 2 nanocomposite pervaporation membranes for ethanol dehydration, Chemical Engineering Science, 64 (2009) 3130-3137.
[23] V. Sencadas, D.M. Correia, C. Ribeiro, S. Moreira, G. Botelho, J.G. Ribelles, S. Lanceros-Méndez, Physical-chemical properties of cross-linked chitosan electrospun fiber mats, Polymer Testing, 31 (2012) 1062-1069.
[24] B.W.S. Souza, M.A. Cerqueira, J.T. Martins, A. Casariego, J.A. Teixeira, A.A. Vicente, Influence of electric fields on the structure of chitosan edible coatings, Food Hydrocolloids, 24 (2010) 330-335.
[25] A. Bojinova, R. Kralchevska, I. Poulios, C. Dushkin, Anatase/rutile TiO2 composites: Influence of the mixing ratio on the photocatalytic degradation of Malachite Green and Orange II in slurry, Materials Chemistry and Physics, 106 (2007) 187-192.

[26] A. Areias, J. Gómez-Tejedor, V. Sencadas, J. Alió, J. Ribelles, S. Lanceros-Mendez, Assessment of parameters influencing fiber characteristics of chitosan nanofiber membrane to optimize fiber mat production, Polymer Engineering & Science, 52 (2012) 1293-1300.
[27] J. Brugnerotto, J. Lizardi, F. Goycoolea, W. Argüelles-Monal, J. Desbrieres, M. Rinaudo, An infrared investigation in relation with chitin and chitosan characterization, Polymer, 42 (2001) 3569-3580.
[28] N. Mohammadpour Dounighi, R. Eskandari, M. Avadi, H. Zolfagharian, A. Mir Mohammad Sadeghi, M. Rezayat, Preparation and in vitro characterization of chitosan nanoparticles containing Mesobuthus eupeus scorpion venom as an antigen delivery system, Journal of Venomous Animals and Toxins Including Tropical Diseases, 18 (2012) 44-52.
[29] J. Kumirska, M. Czerwicka, Z. Kaczyński, A. Bychowska, K. Brzozowski, J. Thöming, P. Stepnowski, Application of spectroscopic methods for structural analysis of chitin and chitosan, Marine drugs, 8 (2010) 1567-1636.
[30] C.d.T. Neto, J. Giacometti, A. Job, F. Ferreira, J. Fonseca, M. Pereira, Thermal analysis of chitosan based networks, Carbohydrate Polymers, 62 (2005) 97-103.
[31] V. Georgieva, D. Zvezdova, L. Vlaev, Non-isothermal kinetics of thermal degradation of chitosan, Chemistry Central Journal, 6 (2012) 81.
[32] V. Sencadas, C.M. Costa, G. Botelho, C. Caparrós, C. Ribeiro, J. Gómez-Ribelles, S. Lanceros-Méndez, Thermal properties of electrospun poly (lactic acid) membranes, Journal of Macromolecular Science, Part B, 51 (2012) 411-424.
[33] G. Wang, L. Xu, J. Zhang, T. Yin, D. Han, Enhanced photocatalytic activity of powders (P25) via calcination treatment, International Journal of Photoenergy, 2012 (2012).
[34] A. Ramaprasad, V. Rao, G. Sanjeev, S. Ramanani, S. Sabharwal, Grafting of polyaniline onto the radiation crosslinked chitosan, Synthetic Metals, 159 (2009) 1983-1990.
[35] J.M. Urreaga, M. De la Orden, Chemical interactions and yellowing in chitosan-treated cellulose, European Polymer Journal, 42 (2006) 2606-2616.
[36] Y. Wang, A. Pitto-Barry, A. Habtemariam, I. Romero-Canelon, P.J. Sadler, N.P. Barry, Nanoparticles of chitosan conjugated to organo-ruthenium complexes, Inorganic Chemistry Frontiers, 3 (2016) 1058-1064.
[37] I.K. Konstantinou, T.A. Albanis, TiO 2-assisted photocatalytic degradation of azo dyes in aqueous solution: kinetic and mechanistic investigations: a review, Applied Catalysis B: Environmental, 49 (2004) 1-14.
[38] D.T. Tran, R. Salmon, Potential photocarcinogenic effects of nanoparticle sunscreens, Australasian Journal of Dermatology, 52 (2011) 1-6.
[39] S. Livraghi, I. Corazzari, M.C. Paganini, G. Ceccone, E. Giamello, B. Fubini, I. Fenoglio, Decreasing the oxidative potential of TiO 2 nanoparticles through modification of the surface with carbon: a new strategy for the production of safe UV filters, Chemical Communications, 46 (2010) 8478-8480.
[40] N. Lakshminarasimhan, A.D. Bokare, W. Choi, Effect of agglomerated state in mesoporous TiO2 on the morphology of photodeposited Pt and photocatalytic activity, The Journal of Physical Chemistry C, 116 (2012) 17531-17539.
[41] V. Vaiano, O. Sacco, D. Sannino, W. Navarra, C. Daniel, V. Venditto, Influence of aggregate size on photoactivity of N-doped TiO 2 particles in aqueous suspensions under visible light irradiation, Journal of Photochemistry and Photobiology A: Chemistry, 336 (2017) 191-197.

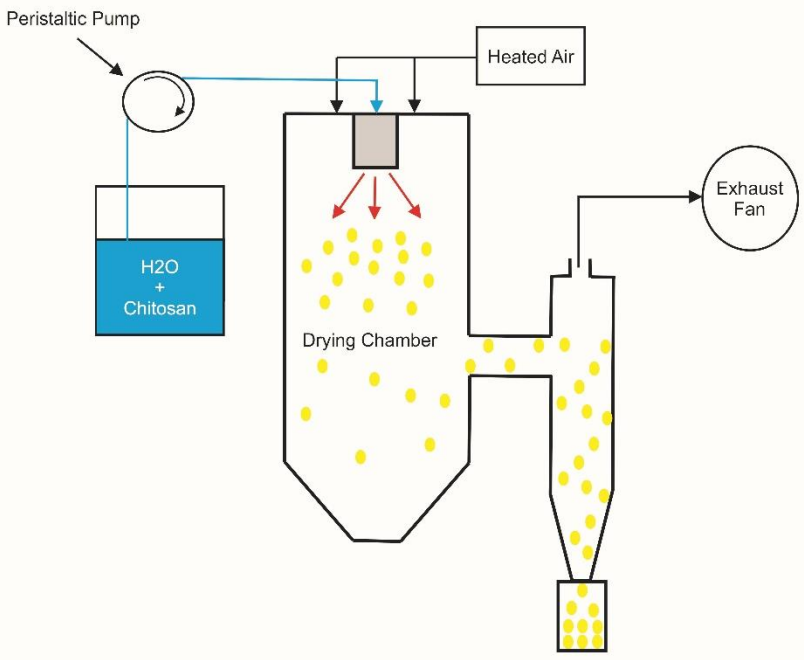

Fig.1. Schematic representation of the home-made spray drying system used.

https://doi.org/10.1016/j.powtec.2018.01.057

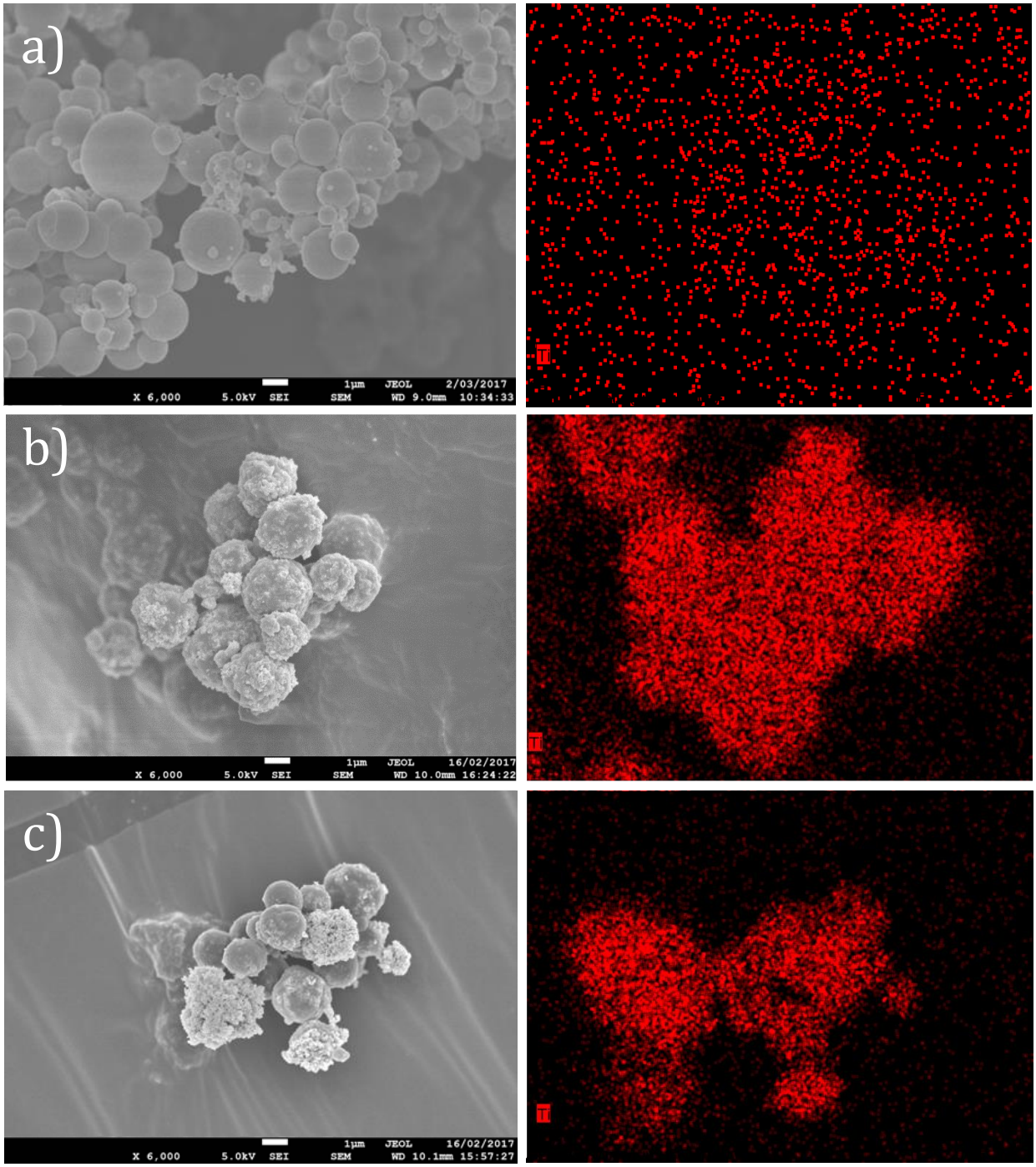

Fig.2. SEM (left) and EDS mapping (right) images for the spray-dried a) CHI, b) 2:1 CHI/TiO_2 and c) 1:1 CHI/TiO_2 particles.

https://doi.org/10.1016/j.powtec.2018.01.057

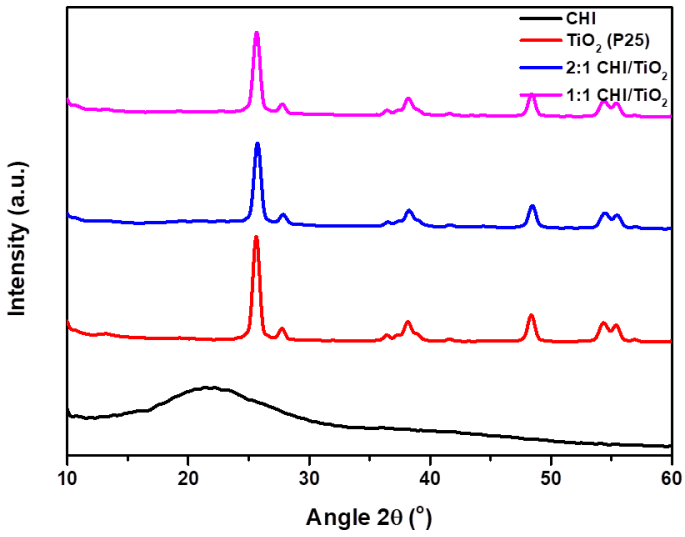

Fig.3. XRD patterns for the raw chitosan starting material, pristine TiO_2 nanoparticles and nanocomposite powders prepared.

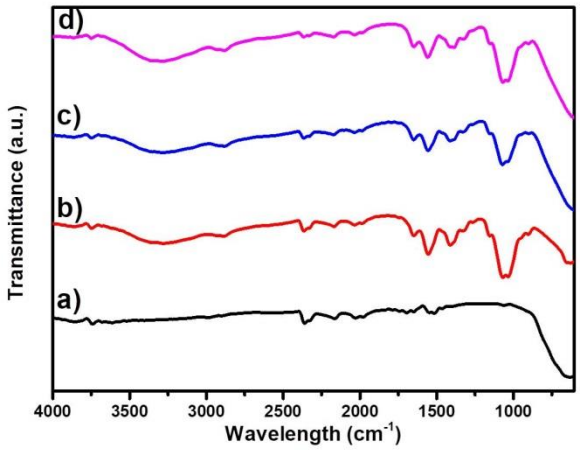

Fig.4. FTIR spectra for the (a) pristine TiO_2 (P25) nanoparticles as well as the spray-dried (b) CHI, (c) 1:1 CHI/TiO_2 and (d) 2:1 CHI/TiO_2 particles.

https://doi.org/10.1016/j.powtec.2018.01.057

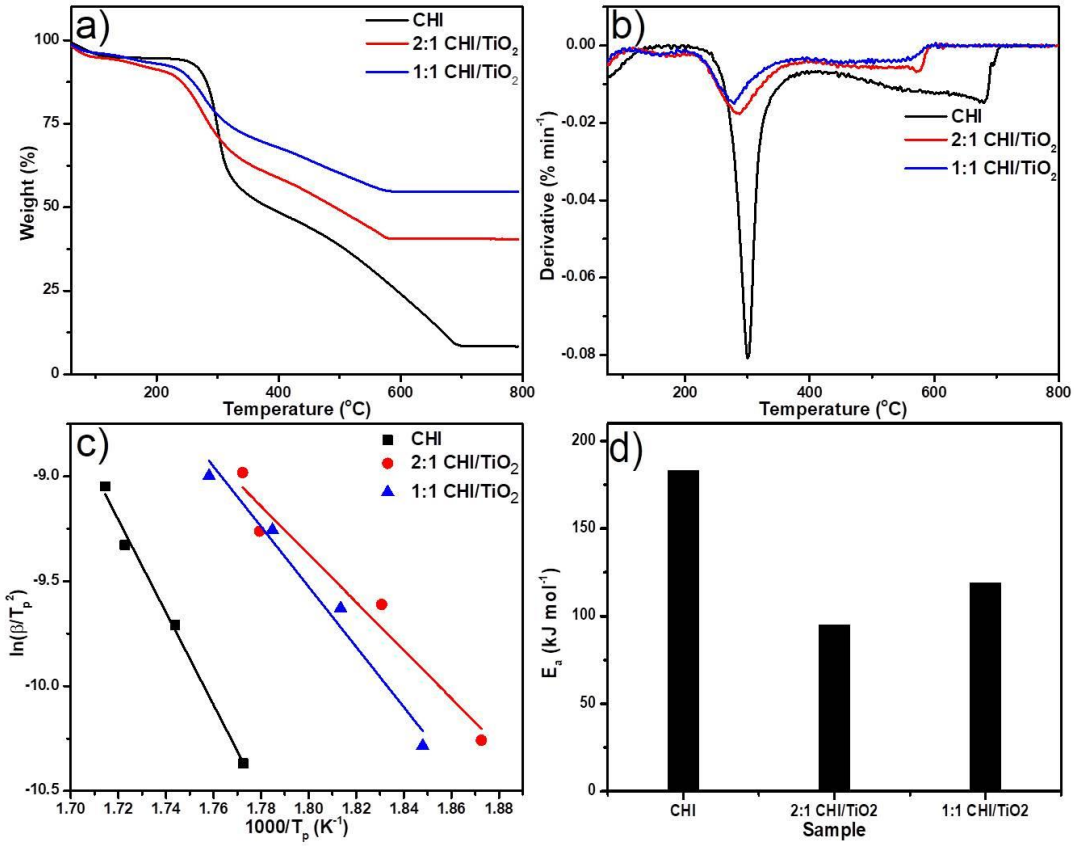

Fig.5. a) TGA curves for the spray-dried samples and corresponding b) derivative curves obtained at a heating rate of 20°C min^{-1}. c) Kissinger plots and influence of chitosan loading on the activation energy (E_a) for the spray-dried materials.

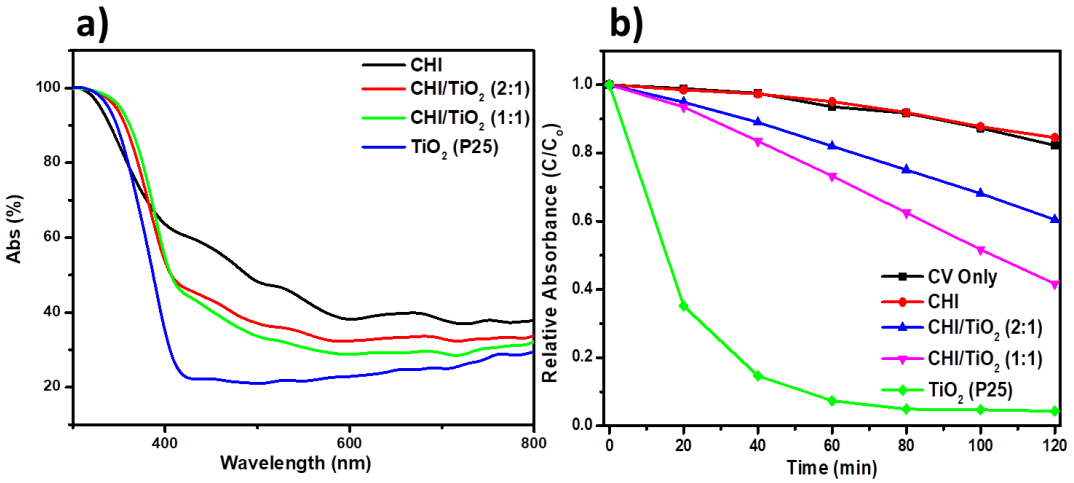

https://doi.org/10.1016/j.powtec.2018.01.057

Fig.6. a) Absorption plots for the spray-dried and commercial samples obtained through diffuse-reflectance spectroscopy. b) Relative decrease in absorbance of crystal violet dye as a function of UV irradiation time in the presence of the spray-dried and commercial samples.

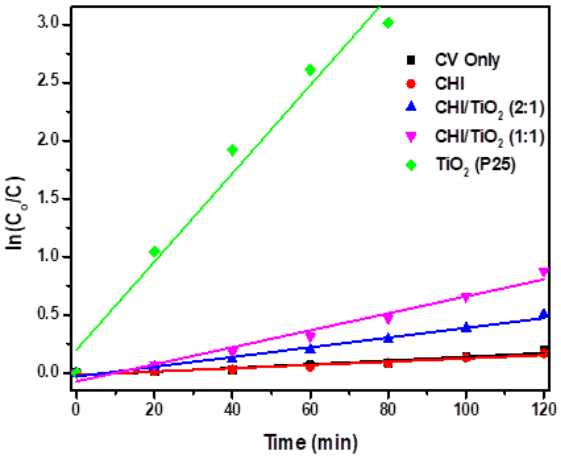

Fig.7. Kinetics plots for the degradation of crystal violet dye as ascribed by the Langmuir-Hinshelwood relationship in the presence of the spray-dried and commercial materials.

Sample	Mean Particle Size (µm)	Coefficient of Variance	T_{onset} (°C)	E_a (kJ mol^{-1})	Residual Mass (%)
CHI	1.4	0.4	279	183	9
2:1 CHI/TiO_2	2.1	0.3	245	95	41
1:1 CHI/TiO_2	2.5	0.3	241	119	55
TiO_2 (P25)	37.2 (nm)	0.6	-	-	-

Table.1. Experimental results obtained from the SEM/TEM and thermal analysis for the spray-dried particles and commercial TiO_2 (P25) nanoparticles.

https://doi.org/10.1016/j.powtec.2018.01.057

Sample	CV degradation (% @120 min)	Rate constant *k* (x 10^{-3})(min^{-1})
CHI	15.5	1.4±0.1
2:1 CHI/TiO_2	39.5	4.2±0.2
1:1 CHI/TiO_2	58.3	7.3±0.5
TiO_2 (P25)	95.7	38.0±0.4

Table.2. Photocatalytic degradation efficiencies and rate constants for the spray-dried particles and commercial TiO_2 (P25) nanoparticles.

https://doi.org/10.1016/j.powtec.2018.01.057